RSC Advances

ROYAL SOCIETY OF CHEMISTRY

www.rsc.org/advances

Perfect Spin-filter, Spin-valve, Switching and Negative Differential Resistance in an Organic Molecular Device with Graphene Leads

Yun Ni[1*], Kai-Lun Yao[2,3], Chao-Qun Tang[1] , Guo-Ying Gao[2] , Hua-hua Fu[2] and Si-cong Zhu[2]

[1]Huazhong University of Science and Technology, Wenhua College, Wuhan, China, 430074.

[2]School of Physics and Wuhan National High Magnetic Field Center, Huazhong University of Science and Technology, Wuhan, China, 430074.

[3]International Center of Materials Physics, Chinese Academy of Science, Shenyang 110015, China

*Corresponding author: niyun@hust.edu.cn

By performing first-principle quantum transport calculations, we proposed a multiple-effect organic molecular device for spintronics. The device is constructed of a perylene tetracarboxylic diimide molecule sandwiched between graphene electrodes. Our calculations show that the device has several perfect spintronics effects such as spin-filter effect, magnetoresistance effect, negative differential resistance effect and spin switching effect. These results indicate that our one-dimensional molecular device is a promising candidate for the future application of graphene-based organic spintronics devices.

Introduction:

Graphene, a single-layered two-dimensional crystal with honeycomb lattice structure, has attracted much attention since the successful fabrication in 2004.[1] Graphene is found to possess many peculiar properties, such as high carrier mobility,[1, 2] long spin relaxation times[3] and room-temperature quantum Hall effect[2], which is very prospective for the potential applications as novel nano-device in electronics and spintronics.[4, 5] Spintronics is a new type of electronics that both the intrinsic properties of electrons, spin and charge, are exploited for electronic applications.[6, 7] By adding the spin degree of freedom, we can use spin-state of the electron to store, carry and read information, which makes spintronics a promising technology to supplement traditional silicon-based electronics.[8, 9] Afterwards the field is rapidly evolving into molecular spintronics,[10, 11] which combines the advantages of spintronics and molecular electronics, where the electron spin can be manipulated in the molecules especially organic molecules.[12, 13] The spin-polarized currents at the molecule level, helps to store more date with less physical space.[14] However, the fabrication of such molecule spintronics device is now hindered by technological difficulties. Recently, molecular devices have been successfully constructed experimentally,[15] where the single organic molecule was sandwiched between graphene electrodes. This finding indicates that it is possible to fabricate organic molecule spintronics device using graphene as the electrode.[16]

As known to all, the infinite sheet of graphene can be cut into two typical graphene nanoribbons (GNRs): armchair-edge GNR (AGNR) and zigzag-edge GNR (ZGNR).[17, 18] Among them, ZGNRs are more notable for its unique edge states and potential applications in spintronic devices such as spin-filter,[19, 20] spin-valve,[21, 22] giant magnetoresistance devices,[23, 24] spin

caloritronic devices.[25, 26] When the edges of ZGNRs are passivated by hydrogen atoms, they have three magnetic states: non-magnetism (NM) state, ferromagnetic (FM) state and anti-ferromagnetic (AFM) state. It has been reported that ZGNR-H have a magnetic insulating ground state with AFM state,[18] and can be magnetized by applying a sufficiently strong magnetic field, leading to a FM state.[9, 23] Recently, R. N. Mahato et al. announced that they found an exceptionally large, room-temperature, small-field magnetoresistance (MR) effect experimentally, in a one-dimensional organic molecular wires system.[27] In addition, the organic molecular wires were composed of perylene tetracarboxylic diimide (PTCDI) derivatives, and the confinement of the current path in molecular systems could lead to a strong increase of the MR. As we know, PTCDI and its derivatives play a role in industry as red to brown dye pigment, and show good n-conducting properties when used as organic semiconductor,[28, 29] which makes them attractive for organic spintronics.

In this paper, we numerically investigate the spin-resolved electron transport for a one-dimensional molecular device, where the PTCDI molecule is sandwiched between two ferromagnetic ZGNR electrodes. Since the spin orientation of the ZGNR electrodes can be adjusted by external magnetic field,[20, 30, 31] the magnetization configuration of the device can be set to parallel configuration (PC, the spin orientation of left and right electrodes are both up) and antiparallel configuration (APC, the spin orientation of left electrode is up and the right one is down). We found that in PC configuration, the transport channel of spin-up is open while the spin-down one is closed at Fermi level, which even reaches 100% spin polarization and is very ideal for spin filters. Moreover, the device shows obvious negative differential resistance (NDR) effect and very large MR. In addition, we can observe an obvious switching effect by changing the

orientation between planes of PTCDI and ZGNRs.

Method and Structure:

The model device we called M1 is illustrated in Figure 1, where the initial orientation of PTCDI plane is coplanar to ZGNR. The left and right electrodes are semi-infinite electrodes respectively, and z direction is the transmission direction. The 6-ZGNR with the number of zigzag carbon chains N=6 is selected as the electrodes.[9] The PTCDI molecule is connected to the 6-ZGNRs through a five-membered carbon ring which is similar to previous research of carbon chains,[20] and all the dangling bonds at the edges are passivated with hydrogen atoms.

Our first-principles calculations are based on the ATOMISTIX TOOLKIT (ATK) package,[32-34] which adopts spin density functional theory combined with nonequilibruim Green's function.[35, 36] The core electrons are described by norm-conserving pseudopotentials, and the local-density approximation (LDA) is used for the exchange-correlation potential.[9, 18, 37] A single-polarized (SZP) basis set is used and the cutoff energy is 150 Ry and a Monkhorst-Pack k-mesh of 1×1×100 is chosen in our work. The structure was optimized before calculation. According to the optimization, the bond distance of C1 and N atoms is about 1.43Å, which is close to the length of carbon-nitrogen single bond, so we believe the covalent bond type of C1 and N atoms is σ -bond. The convergence parameters of the optimization were chosen as follows: total energy tolerance 1×10^{-5} eV/atom, maximum force tolerance 0.05eV/Å. The vacuum layers between two sheets along x and y directions (defined in Figure. 1) are more than 10Å. The NEGF-DFT self-consistency is controlled by a numerical tolerance of 10^{-5}eV. The integration grid of current calculation is 10×10. The spin-dependent current through the system is calculated using

the Landauer formula:

$$I^{\uparrow(\downarrow)} = \frac{e}{h}\int_{-\infty}^{\infty}\{T^{\uparrow(\downarrow)}(E)[f_L(E,\mu) - f_R(E,\mu)]\}dE \quad , \qquad (1)$$

where $f_{L(R)}(E,\mu)$ is the equilibrium Fermi distribution for the left (right) electrode, and $\mu_{L,R}=E_F \pm eV/2$ is the electrochemical potentials of the left and right electrodes in terms of the common Fermi energy E_F, and $T^{\uparrow(\downarrow)}(E)$ is the spin-resolved transmission defined as

$$T^{\uparrow(\downarrow)}(E) = Tr[\Gamma_L G^R \Gamma_R G^A]^{\uparrow(\downarrow)} \quad , \qquad (2)$$

where $G^{R(A)}$ is the retarded (advanced) Green's functions of the central region and $\Gamma_{L(R)}$ is the coupling matrix of the left(right) electrode.

Result and Discussion:

The calculated spin-resolved electron transmission spectra of the device in PC and APC magnetization configuration without any external electrical fields are shown in Figure 2(a) and (b). It can be seen obviously that in both PC and APC configurations the transmission spectra are spin-polarized, and the spin-up ones are generally larger than spin-down ones. We also see that the spin-up spectrum has a broad peak near the Fermi level in PC, and splits to both sides of the Fermi level in APC. On the other hand, for the spin-down one, the positions of the transmission peaks are little changed from PC to APC, except for some small deviations of the values and the tiny peak at 0.05ev in PC. It is noteworthy that in PC the spin-up transmission channel is open while the spin-down one is blocked at the Fermi level, which originates from the differences in local density of states (LDOS) of the Fermi level, as shown in Figure 2(c) and (d). The LDOS of the spin-up one decreases from both sides to the middle but remains large on the PTCDI molecule, providing the channels for transmission. However, the LDOS of the spin-down one nearly vanished on the

PTCDI molecule and virtually no channel helps to the transport of the electrons. Therefore, the spin-polarization of the device approaches 100% around Fermi level in PC case at zero bias, which is a perfect spin-filter. Then we provide a small bias (<0.2V) to the device, and the spin-depended currents and the spin-polarization was shown as well (Figure 3a, b and c). Since the structure of our devices is symmetric, we only concentrate on the case of positive bias. Note that when the bias is zero, the spin-polarization is defined as $SP= (T_{up}-T_{down})/ (T_{up}+T_{down}) \times 100$; while with non-zero bias, the spin-polarization is calculated by $SP= (I_{up}-I_{down})/ (I_{up}+I_{down}) \times 100$. In PC condition, the spin-polarizations are quite large, obviously higher than 95%, except for some individual data around 90%. Moreover, the spin-polarizations decrease with the bias increasing on the whole, and the highest spin-polarization occurs at zero bias. In APC condition, the spin-polarizations are quite smaller than PC. That's because both the spin-up and spin-down transmission channels are blocked in this configuration, in according with the LDOS results of the spin-up and spin-down electrons in figure 2(e) and (f).

From the spin-resolved I-V curves of our device within 0.2V in different magnetization configuration (Figure 3a), we can also find some singular points like the 0.18V of PC and 0.15V of APC for the spin-up currents. We would like to take the spin-up one in PC case for example to explain the cause of the singular point. The inset of figure3a shows the current curve with smaller spaced point in the vicinity of 0.18V. We can see that the current suddenly dive down at 0.175V, and then the curve keeps low and changes very little until 0.186V, where the current sharply increases and keeps high. As we know, the transport properties of a molecular device are determined by the electronic structures, especially the energy position of molecular orbital, which provide transmission channels for the electron tunneling. In order to see the variation of the

molecular orbital more clearly, we plotted the bias-dependent evolutions of LUMO (lowest unoccupied molecular orbital), HOMO (highest occupied molecular orbital), LUMO+1 and HOMO-1. Since the molecular orbital is close on each voltage from 0.175V to 0.185V, we take the case of 0.18V as representative to show it. Seen from Figure 3d, the energy was chosen from -0.3ev to 0.3ev, the triangular region surrounded by the intersecting dashed lines is referred to the bias window, and the energy data are molecular projected self-consistent Hamiltonian (MPSH) eigenvalues. As we know, only the Energy Levels located in bias window contribute to the transport. It can be clearly seen that the HOMO-LUMO gap is decreased gradually with the increasing bias from 0V to 0.15V, so the current rises linearly and stably in this region. When the bias reaches 0.16V, although the HOMO-LUMO gap has no obviously change, the HOMO orbital raises and is very close to the Fermi level, resulting in a large increase of the current at 0.16V (Figure3a). At 0.18V, the current suddenly drops down also can be explained by the molecular orbital in figure3d. The LUMO orbital at 0.18V ascends a major step not only increases the HOMO-LUMO gap greatly but also goes beyond the region of bias window. Meanwhile, the HOMO-1 orbital enters the bias window, but the MPSH eigenstate for the HOMO-1 at 0.18V (Figure3e) shows that they are highly localized at the right electrode area, giving no contribution to the electron transport. Therefore, the current around 0.18V is very small (from 0.175V to 0.185V) in the spin-up I-V curve of PC. For spin-down case and APC configuration, the variation of the I-V curves can also be analyzed in the same way.

Also, we investigate the magnetoresistance (MR) of the device changing from PC to APC magnetization configuration, which can be obtained from the equation MR (%) = $(R_{AP}-R_P)/(R_P)$ $\times 100$, where R_{AP} and R_P are the resistances in the APC and PC configuration. Note that when the

bias is zero, the MR can be calculated by the transmission coefficient of the spin-up and spin-down electrons in PC and APC, which is MR (%) = $[(T_{AP\text{-}up}+T_{AP\text{-}down})^{-1}-(T_{P\text{-}up}+T_{P\text{-}down})^{-1}]$ $/(T_{P\text{-}up}+T_{P\text{-}down})^{-1} \times 100$. While with non-zero bias, the MR is obtained from the total currents of PC and APC, which is MR (%) = $[(I_{PC}- I_{APC})/ I_{APC}] \times 100$. Figure 4a shows the bias-dependent MR of the device. The maximum value of the MR occurs at zero bias and is nearly 10^4 %, yet it decreases quickly with the rise of bias. Within small bias, when the bias reaches 0.1V, the MR drops to about 10^3 %, and is still larger than that of conventional metal-based MR devices. The large MR effect is mainly caused by the selective transmission of the spin-resolved electrons in the device, and is very significant for fabricating efficient graphene-based spin-valve devices.

Next, we investigate the spin-resolved currents of a larger bias (less than 1.0V), and the corresponding I-V curves are shown in Figure 4b. It can be obviously seen that both in PC and APC configuration the currents are spin-polarized, and the spin-polarization of PC is generally larger than APC. It is noteworthy that some of the curves show obvious NDR effect, among which the spin-up one of PC configuration is the most significant. Thus with this case as representation, we will thoroughly investigate the formation mechanism of the NDR effect. First, we present the spin-up transmission spectra around the Fermi level in figure 5, and the bias is selected from 0.3V to 0.8V, since the NDR effect mainly occurs within this region. The comparison of the transmission spectra at bias 0.3V and 0.7V shows that with the bias window expanding the spin-up spectrum varies greatly: the peak above the Fermi level shrinks and shifts away from the Fermi level; the spectrum below the Fermi level gradually appears a sharp peak at about -0.15ev. From Eq.1, we know that the current is determined by the corresponding integral areas of the transmission spectra in the bias window. However, we can't judge the values of spectrum integral

areas at 0.3V and 0.7V intuitively, since the variation of the spectra is quite complex. In order to see the cause of the NDR effect more intuitively, we have investigated the bias-dependent evolutions of several molecular orbitals near the Fermi level, and the MPSH eigenvalues are shown in figure 6a. It can be obviously seen that when the bias reaches 0.4V, the HOMO descends but the LUMO ascends, leading to a dramatically increase of the HOMO-LUMO gap. Simultaneously, seen from the MPSH eigenstates of the HOMO and LUMO orbitals at bias 0.3V and 0.4V (Figure 6b-e), the distribution of HOMOs are almost the same, throughout the PTCDI molecule, providing the channels for transmission. However for the LUMOs, the MPSH eigenstates at bias 0.4V are more localized than 0.3V. That's why the NDR effect occurs at 0.4V. When the bias reaches 0.7V, the current gets a valley and then rises rapidly at 0.8V. As shown in figure 6a, from 0.7V to 0.8V, both HOMO and LUMO descends, and the LUMO locates very close to the Fermi level at 0.8V despite the slightly increase of HOMO-LUMO gap. Meanwhile we can also observe from the MPSH eigenstates of HOMO and LUMO at bias 0.7V and 0.8V (Figure 6f-i). The distributions of HOMOs are both throughout the PTCDI molecule, but the LUMOs are quite different. The LUMOs are quite localized at right electrode of bias 0.7V but distributed throughout the centre region of 0.8V, so the current rises significantly when the bias goes from 0.7V to 0.8V.

Finally, we consider another configuration of the PTCDI molecule and the GNR leads, which is shown in figure 7 and defined as M2. The orientation of PTCDI plane is perpendicular to ZGNR, which may be reversed from M1 (figure 1) by thermal activation, micromechanical operation and electric field.[38-41] The calculated spin-dependent currents of M1 and M2 both in PC and APC are shown in figure 8a and b, where we can see clearly that the currents of M2 are rather smaller

comparing with that of M1. That is to say, the spin-resolved currents can be controlled by changing the orientation between planes of PTCDI molecule and the GNR leads. When the planes are coplanar, the molecular device is on; when the planes are perpendicular, the molecular device is off. The corresponding ON/OFF switch ratios are displayed in figure 8c and d. For most bias within 1.0V, the ON/OFF ratios are dramatically high, in which the highest one even attains 10^5 for spin-up condition at 0.2V in APC. The ratios are quite large but not steady, which need to be improved further. The huge ratio is caused by the mismatch between p_y channel of PTCDI molecule and the π-orbital of GNR in perpendicular configuration, resulting in nearly no channel for electron transmission. The outstanding switching effect makes the device possible to achieve ideal spin switching device, which plays an important role in the application of spintronics.

Conclusions:

In conclusion, we proposed a one-dimensional molecular device of PTCDI molecule sandwiched between ZGNR leads. These devices could generate extremely high spin-polarization under small bias (zero bias even 100%) due to the large spin-filter at the Fermi level. Moreover, the spin-polarized currents and large magnetoresistance are obtained by controlling the external magnetic direction of the electrodes. In addition, the obvious NDR effects are observed in our results with the extension of the bias, which are mainly caused by the variations of the molecular orbital. Furthermore, the molecular switch can be theoretically realized with dramatically large ON/OFF switch ratios by mechanically changing the orientation between the PTCDI and ZGNRs. All in all, the molecular device shows varies of important properties of spintronics, and can be served as perfect spin-filter, spin-valve, and spin switching etc., which holds the promise of new multiple-effect devices for spintronics.

Acknowledgments

This work was supported by the National Natural Science Foundation of China under Grants No. 11274130，No. 11074081.

Reference

1. K. S. Novoselov, A. K. Geim, S. Morozov, D. Jiang, Y. Zhang, S. Dubonos, I. Grigorieva and A. Firsov, *Science*, 2004, **306**, 666.
2. Y. Zhang, Y.-W. Tan, H. L. Stormer and P. Kim, *Nature*, 2005, **438**, 201.
3. A. K. Geim and K. S. Novoselov, *Nature materials*, 2007, **6**, 183.
4. A. C. Neto, F. Guinea, N. Peres, K. S. Novoselov and A. K. Geim, *Reviews of modern physics*, 2009, **81**, 109.
5. W. L. Wang, S. Meng and E. Kaxiras, *Nano Letters*, 2008, **8**, 241.
6. I. Žutić, J. Fabian and S. D. Sarma, *Reviews of modern physics*, 2004, **76**, 323.
7. S. Wolf, D. Awschalom, R. Buhrman, J. Daughton, S. Von Molnar, M. Roukes, A. Y. Chtchelkanova and D. Treger, *Science*, 2001, **294**, 1488.
8. D. D. Awschalom and M. E. Flatté, *Nature Physics*, 2007, **3**, 153.
9. Y.-W. Son, M. L. Cohen and S. G. Louie, *Nature*, 2006, **444**, 347.
10. L. Bogani and W. Wernsdorfer, *Nature materials*, 2008, **7**, 179.
11. A. R. Rocha, V. M. Garcia-Suarez, S. W. Bailey, C. J. Lambert, J. Ferrer and S. Sanvito, *Nature materials*, 2005, **4**, 335.
12. W. Naber, S. Faez and W. Van der Wiel, *Journal of Physics D: Applied Physics*, 2007, **40**, 205.

13. W. Xu, G. Szulczewski, P. LeClair, I. Navarrete, R. Schad, G. Miao, H. Guo and A. Gupta, *Applied physics letters*, 2007, **90**, 072506.

14. S. Sanvito, *Nature Physics*, 2010, **6**, 562.

15. F. Prins, A. Barreiro, J. W. Ruitenberg, J. S. Seldenthuis, N. Aliaga-Alcalde, L. M. Vandersypen and H. S. van der Zant, *Nano Letters*, 2011, **11**, 4607.

16. J. Li, Z. Zhang, J. Zhang, W. Tian, Z. Fan, X. Deng and G. Tang, *Organic Electronics*, 2013, **14**, 958.

17. K. Nakada, M. Fujita, G. Dresselhaus and M. S. Dresselhaus, *Physical Review B*, 1996, **54**, 17954.

18. Y.-W. Son, M. L. Cohen and S. G. Louie, *Physical Review Letters*, 2006, **97**, 216803.

19. J. Nakabayashi, D. Yamamoto and S. Kurihara, *Physical Review Letters*, 2009, **102**, 066803.

20. M. Zeng, L. Shen, Y. Cai, Z. Sha and Y. Feng, *Applied physics letters*, 2010, **96**, 042104.

21. N. Tombros, C. Jozsa, M. Popinciuc, H. T. Jonkman and B. J. Van Wees, *Nature*, 2007, **448**, 571.

22. S. Cho, Y.-F. Chen and M. S. Fuhrer, *Applied physics letters*, 2007, **91**, 123105.

23. W. Y. Kim and K. S. Kim, *Nature nanotechnology*, 2008, **3**, 408.

24. J. Bai, R. Cheng, F. Xiu, L. Liao, M. Wang, A. Shailos, K. L. Wang, Y. Huang and X. Duan, *Nature nanotechnology*, 2010, **5**, 655.

25. M. Zeng, Y. Feng and G. Liang, *Nano Letters*, 2011, **11**, 1369.

26. Y. Ni, K. Yao, H. Fu, G. Gao, S. Zhu and S. Wang, *Scientific reports*, 2013, **3**, 1380.

27. R. Mahato, H. Lülf, M. Siekman, S. Kersten, P. Bobbert, M. de Jong, L. De Cola and W. van der Wiel, *Science*, 2013, **341**, 257.

28. P. R. Malenfant, C. D. Dimitrakopoulos, J. D. Gelorme, L. L. Kosbar, T. O. Graham, A. Curioni and W. Andreoni, *Applied physics letters*, 2002, **80**, 2517.

29. D. Lehmann and D. R. Zahn, *Applied Physics A*, 2009, **95**, 203.

30. H. Wan, B. Zhou, X. Chen, C. Q. Sun and G. Zhou, *The Journal of Physical Chemistry C*, 2012, **116**, 2570.

31. Y. Ni, K.-L. Yao, H.-H. Fu, G.-Y. Gao, S.-C. Zhu, B. Luo, S.-L. Wang and R.-X. Li, *Nanoscale*, 2013, **5**, 4468.

32. J. Taylor, H. Guo and J. Wang, *Physical Review B*, 2001, **63**, 245407.

33. M. Brandbyge, J.-L. Mozos, P. Ordejón, J. Taylor and K. Stokbro, *Physical Review B*, 2002, **65**, 165401.

34. J. M. Soler, E. Artacho, J. D. Gale, A. García, J. Junquera, P. Ordejón and D. Sánchez-Portal, *Journal of Physics: Condensed Matter*, 2002, **14**, 2745.

35. H.-H. Fu and K.-L. Yao, *Applied Physics Letters*, 2012, **100**, 013502.

36. H.-H. Fu and K.-L. Yao, *The Journal of chemical physics*, 2011, **134**, 054903.

37. O. V. Yazyev and L. Helm, *Physical Review B*, 2007, **75**, 125408.

38. M. Vergniory, J. Granadino-Roldan, A. Garcia-Lekue and L.-W. Wang, *Applied Physics Letters*, 2010, **97**, 262114.

39. R. Pati and S. P. Karna, *Physical Review B*, 2004, **69**, 155419.

40. T. Martins, A. Fazzio and A. J. da Silva, *Physical Review B*, 2009, **79**, 115413.

41. E. Malic, C. Weber, M. Richter, V. Atalla, T. Klamroth, P. Saalfrank, S. Reich and A. Knorr, *Physical review letters*, 2011, **106**, 097401.

Figures captions:

Figure 1. (Color online) A schematic device model of PTCDI molecule bridging two zigzag graphene nanoribbon leads. The red frame indicates the left leads while the blue one indicates the right leads. The scattering region includes the PTCDI molecule and the surface layers. The transmission direction is along z direction.

Figure 2. (Color online) The spin-dependent electron transmission spectra at zero bias in (a) PC and (b) APC configuration. The spin-resolved LDOS at the Fermi level is shown in (c, d) for PC and (e, f) for APC. The isovalues of (c)-(f) are 0.001 a.u.

Figure 3. (Color online) (a) The spin-resolved I-V curves for PC and APC configuration within bias 0.2V. (b) and (c) shows the spin polarization of PC and APC. (d) The bias-dependent evolution of molecular orbitals for the spin-up one within 0.2V in PC configuration. (e) The eigenstate distribution of the HOMO-1 orbital at 0.18V, the isovalues is 0.02 a.u. The inset of figure3a shows the current curve with smaller spaced point in the vicinity of 0.18V.

Figure 4. (Color online) (a) The magneto-resistance of the device. (b) The spin-resolved I-V curves for PC and APC configuration within bias 1.0V.

Figure 5. (Color online) The spin-dependent transmission spectra of the device at bias (a) 0.3V, (b) 0.4V, (c) 0.5V, (d) 0.6V, (e) 0.7V and (f) 0.8V in PC configuration.

Figure 6. (Color online) (a) The bias-dependent evolution of molecular orbitals for the spin-up one within 1.0V in PC configuration. (b)-(i) shows the eigenstate distribution of HOMO and LUMO at bias 0.3V, 0.4V, 0.7V and 0.8V, the isovalues are all 0.005 a.u.

Figure 7. (Color online) Schematic of the switching device when the orientation of PTCDI plane is perpendicular to ZGNR plane.

Figure 8. (Color online) The spin-resolved I-V curves for M1(ON) and M2(OFF) in (a) PC and (b) APC configuration. (c) and (d) shows ON/OFF switch ratios in PC and APC.

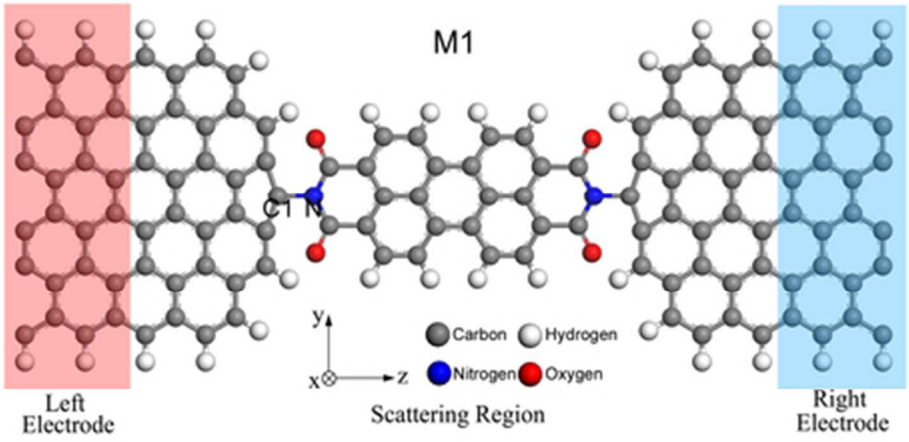

A schematic device model of PTCDI molecule bridging two zigzag graphene nanoribbon leads. The red frame indicates the left leads while the blue one indicates the right leads. The scattering region includes the PTCDI molecule and the surface layers. The transmission direction is along z direction.
41x20mm (300 x 300 DPI)

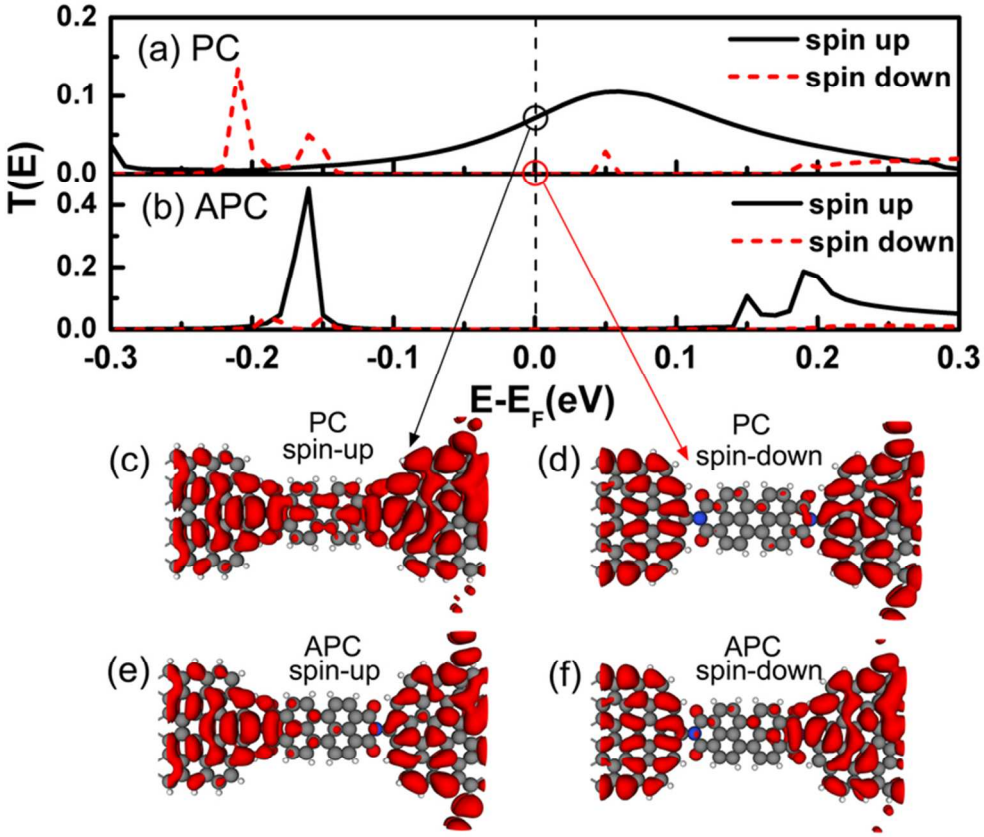

The spin-dependent electron transmission spectra at zero bias in (a) PC and (b) APC configuration. The spin-resolved LDOS at the Fermi level is shown in (c, d) for PC and (e, f) for APC. The isovalues of (c)-(f) are 0.001 a.u.
71x61mm (300 x 300 DPI)

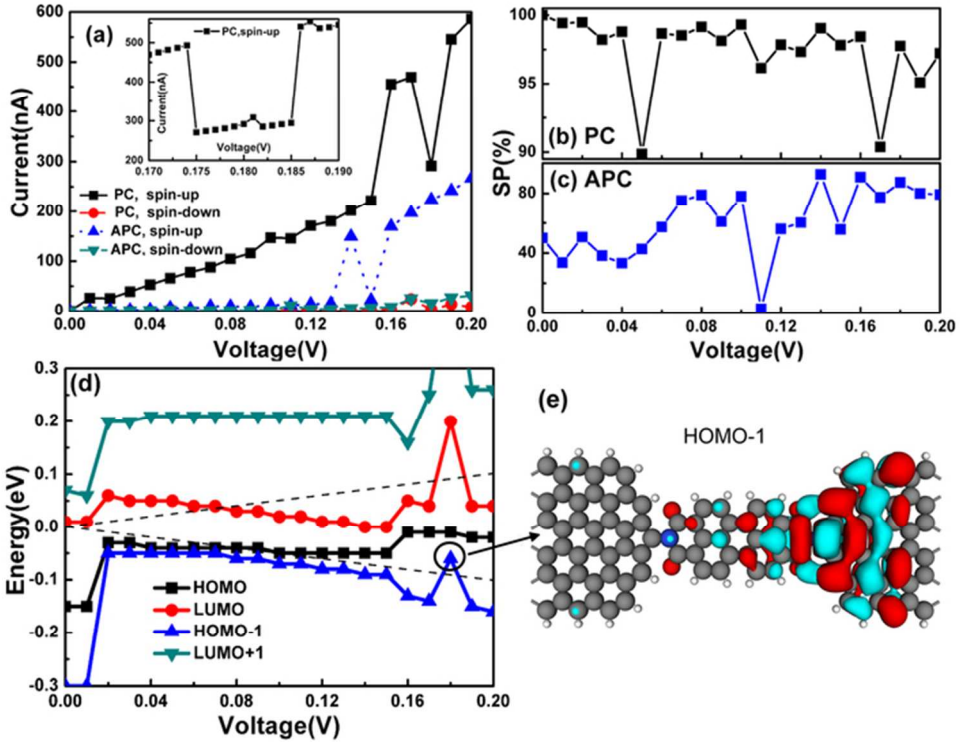

(a) The spin-resolved I-V curves for PC and APC configuration within bias 0.2V. (b) and (c) shows the spin polarization of PC and APC. (d) The bias-dependent evolution of molecular orbitals for the spin-up one within 0.2V in PC configuration. (e) The eigenstate distribution of the HOMO-1 orbital at 0.18V, the isovalues is 0.02 a.u. The inset of figure3a shows the current curve with smaller spaced point in the vicinity of 0.18V.
62x46mm (300 x 300 DPI)

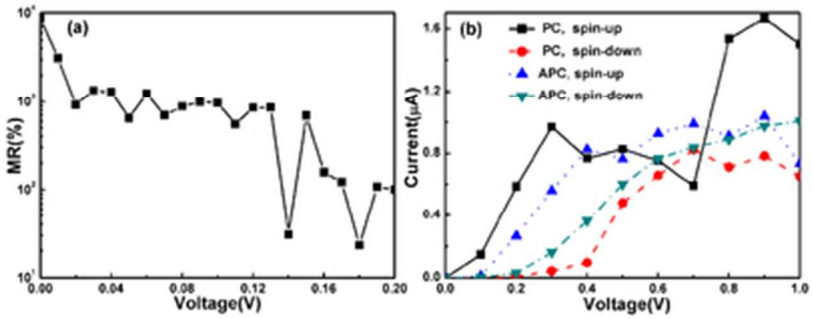

(a) The magneto-resistance of the device. (b) The spin-resolved I-V curves for PC and APC configuration within bias 1.0V.
34x14mm (300 x 300 DPI)

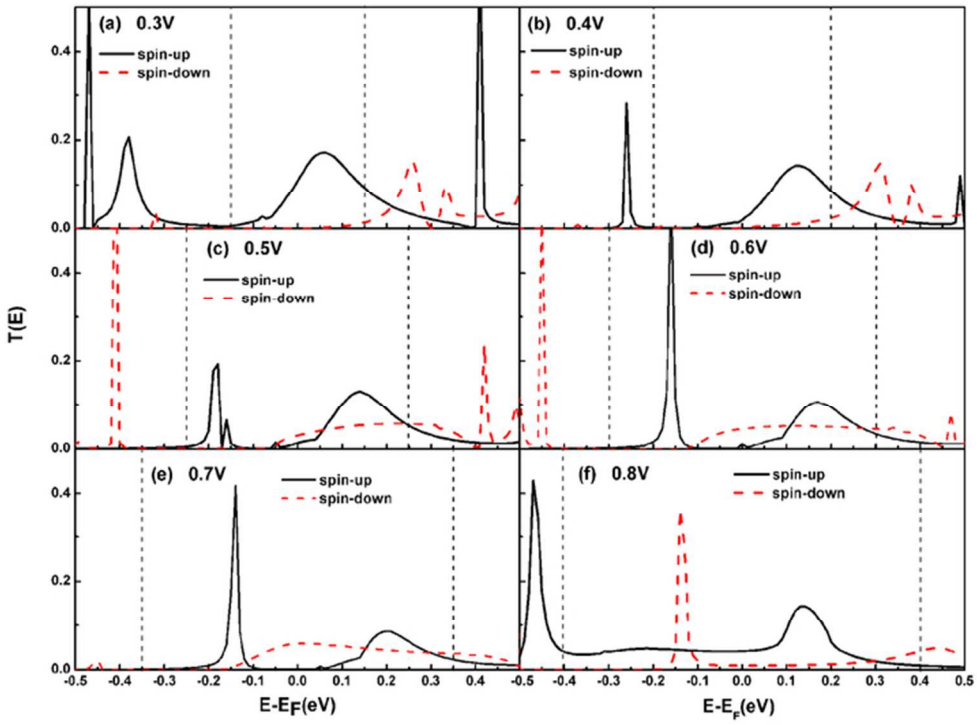

The spin-dependent transmission spectra of the device at bias (a) 0.3V, (b) 0.4V, (c) 0.5V, (d) 0.6V, (e) 0.7V and (f) 0.8V in PC configuration.
62x46mm (300 x 300 DPI)

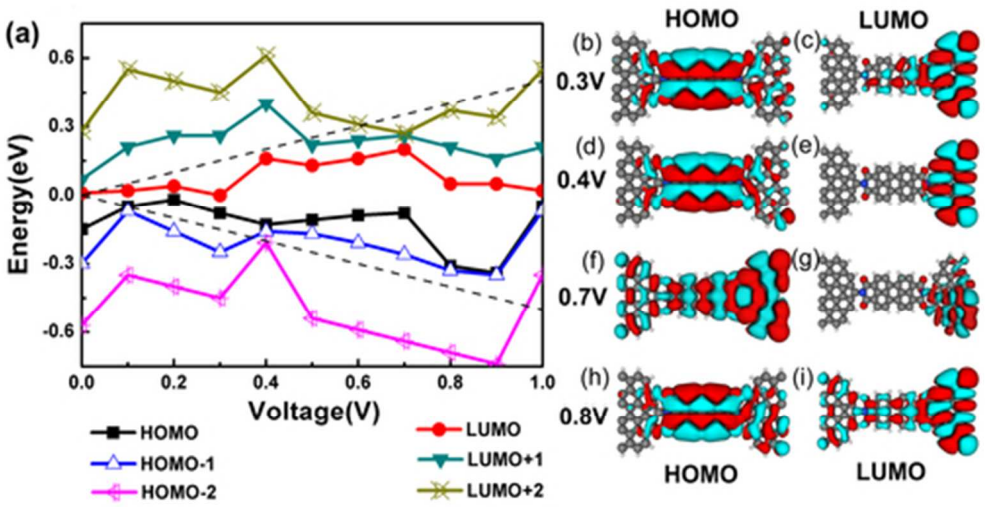

(a) The bias-dependent evolution of molecular orbitals for the spin-up one within 1.0V in PC configuration. (b)-(i) shows the eigenstate distribution of HOMO and LUMO at bias 0.3V, 0.4V, 0.7V and 0.8V, the isovalues are all 0.005 a.u.
43x22mm (300 x 300 DPI)

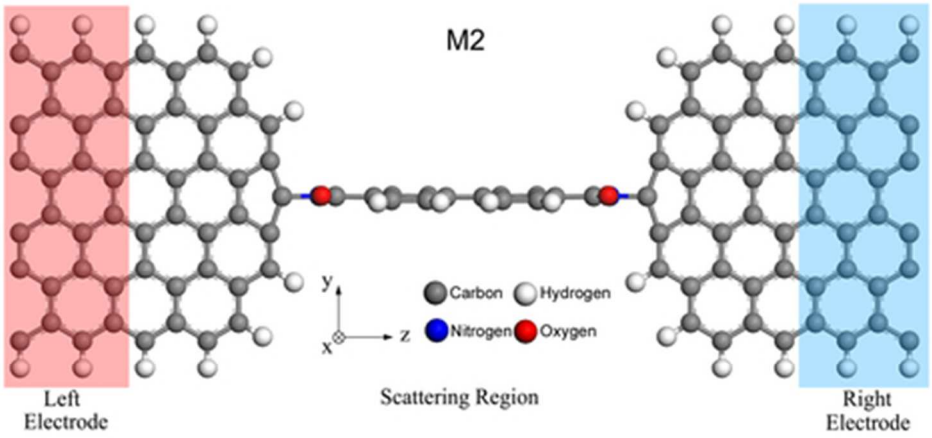

Schematic of the switching device when the orientation of PTCDI plane is perpendicular to ZGNR plane.
40x19mm (300 x 300 DPI)

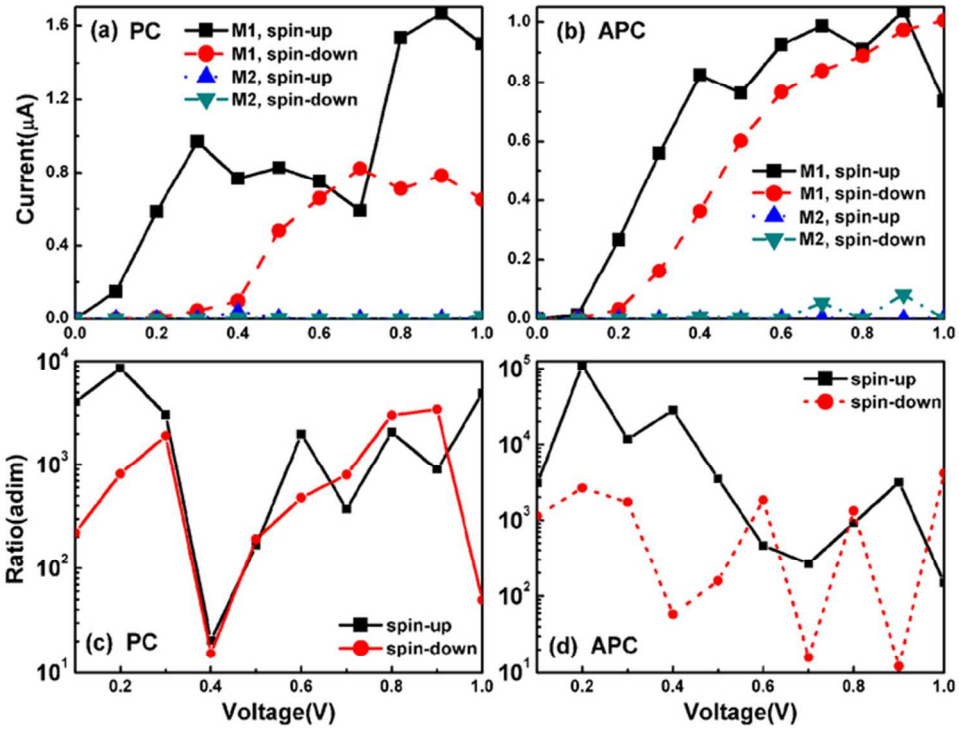

The spin-resolved I-V curves for M1(ON) and M2(OFF) in (a) PC and (b) APC configuration. (c) and (d) shows ON/OFF switch ratios in PC and APC.
63x48mm (300 x 300 DPI)